CAN WE ASSESS LANDSLIDE HAZARDS IN THE VOLCANIC CRATER OF LAKE ALBANO, ROME, ITALY?

ANTONIO PATERA[1*] & ANDREA FABBRI[2†]
[1]Istituto Nazionale di Geofisica e Vulcanologia, Italy
[2]Dipartimento di Scienze dell'Ambiente e della Terra, Università di Milano-Bicocca, Italy

ABSTRACT

This study applies mathematical models for assessing landslide susceptibility around Lake Albano, a volcanic crater and resort area near the city of Rome, Italy. The hazards are mass movements of many different types, recorded for more than 2,100 years that continue occurring to date encroaching with expanding urbanization and socioeconomic activities. The study area surrounding the lake occupies 30 km^2, in the form of a digital raster of 1002 pixels × 1202 lines at 5 m resolution: 975,093 above the water level and 229,311 below it. Of those, 8,867 pixels indicate the location of 150 sub-aerial landslides and 34,028 pixels that of 65 sub-aqueous landslides, respectively, that is, high densities of mass movements. A database collected the most available information on the landslides: distributions, types, linear and polygonal forms, and sub-aerial or sub-aqueous locations. Digitized categorical maps of land use classes and lithology units, in addition to a continuous field of high-resolution topographic elevation data, represented their physical settings. From a dense grid of elevation points, continuous-value maps at 5 m resolution were the following: aspect, digital elevation model, slope, curvature, planform, and profile. The results of prediction modelling by a fuzzy set membership function and a logistic discriminant function were digital images ranking the study area into relative levels of susceptibility. The spatial support of the settings varied with landslide types and physiographic conditions. The levels integrated empirical likelihood values representing the contrast in settings for all the pixels in the presence of the landslides with the pixel in their absence for each landslide type within the study area. Such ranks tend to overlap in predictions from the two models and for different types of landslides. Predicting landslide susceptibility for the area is feasible and with low uncertainty; however, the volcanic and socioeconomic context is a main challenge to measures of hazard and risk avoidance.
Keywords: landslide susceptibility, volcanic crater, fuzzy sets, logistic discriminant functions, spatial support, prediction modelling.

1 INTRODUCTION

Lake Albano has represented a focus of attention since prehistoric times. The lake, located approximately 20 km from the metropolitan centre of Rome, has a volcanic origin. Geologically it belongs to the Quaternary volcanic district of the Colli Albani (Albani Hills). The volcanic setting hosting the lake shows inward inclined flanks and steep slopes over the internal walls of the crater where a multitude of slope failures have been and are taking place.

Due to its natural beauty and the vicinity to the city a variety of recreational activities and urbanizations have developed along the internal slopes of the crater and the edge of the coastline. They represent elements exposed not only to the high risk of slope instability but also to tsunamis waves as secondary effects of sub-aqueous landslides. Patera and Fabbri [1], provided a synthesis of the geology and geomorphology settings of the Colli Albani and Lake Albano. This is summarised here.

Hydrothermal circulation, seismicity, and uplifting are signs of volcanic activity in the volcanic complex of the Colli Albani. What is left of three eruptive phases of 600,000–350,000 years ago, 350,000–270,000 years ago, and 200,000 years ago, respectively, is a

* *ORCID: https://orcid.org/0000-0001-7641-4689*
† *ORCID: https://orcid.org/0000-0002-9055-5960*

WIT Transactions on The Built Environment, Vol 214, © 2022 WIT Press
www.witpress.com, ISSN 1743-3509 (on-line)
doi:10.2495/SSR220011

final hydro-magmatic phase to the present. The last eruptive centre appears to be Lake Albano that produced slag deposits of 36,000 years of age, recent deposits of mudslides of 5,800 years ago and the flood of 398 BC, possibly a consequence of the injection of hot fluids rich in CO_2 [2]. Furthermore, many emissions of gas, H_2S and CO_2, are a main cause of natural hazard associated to the volcanic activity [3], [4].

The edge of the crater reaches various elevations ranging from 585 m to a minimum of 390 m.a.s.l. while the coastline is at approximately 290 m.a.s.l. Depth of the lake is 167 m and its surface area is about 6 km^2. The lake sediments completely cover the lake bottom with thickness up to 14 m. Observed were hiatus in sediments, variation of $CaCO_3$ deposition rates, lake level fluctuations, uplift of the soil and paroxysmal degassing phenomena.
Within the crater, three large platforms were identified as follows. The first forms the actual beach, and reaches 10 to 20 m below the water level interrupted by an 80 m escarpment. The second is ring shaped at the centre-south of the lake leading to a second escarpment of 35–50 m. The third is at the bottom of the lake at 126–133 m.a.s.l. [5].

The presence of a potentially active volcano in a densely populated area like the metropolitan Rome has led various researchers to evaluate volcanic risk in a multitude of studies on monitoring the gases dissolved in the lake, landslide risk in the internal slopes of Lake Albano including tsunamis risk of particular impact on an enclosed basin [5]–[7].

To account for the continued slope failure activity at Lake Albano, a simple Web query, such as “frane sul Lago Albano” (landslides on Lake Albano), returns pieces of news on local media on landslides just occurred on the following dates: 21 February 2011, 22 March 2011, 30 November 2014, 23 February 2015, 22 December 2015, 28 January 2016, 14 September 2017, 14 January 2018 and 28 September 2020. In addition, a query like “landslides on Lake Albano” returns a multitude of scientific papers about landslide studies concerning the lake. Furthermore, various social and cultural activities are taking place concerning Lake Albano and its protection. A list and description of their websites is in the Appendix. It testifies to the high degree of socioeconomic and environmental concern of the local communities.

Encouraged by the visible scientific and social interest in studying and protecting the lake area and the communities living around the lake, or touring it to enjoy its amenities, we have collected available data constructing a digital database. Its purpose is spatial prediction modelling of landslide susceptibility in the Lake Albano surroundings. Following a pilot study to document the database, its quality and suitability for predictive modelling [1], our analysis attempts to provide interpretable and robust assessments of a high density area of landslides occurrences in both the sub-aerial and the sub-aqueous settings. With a high density of events and a variety of dynamic types of landslides, can we provide acceptable and useable assessments?

To provide answers to this question, the following sections describe the database, introduce concepts and models, and discuss experiments leading to *prediction patterns* expressing the likelihood or possibility of future landslide occurrences estimated from the available data. We finally point out the limitations and complexities of the task.

2 THE DATABASE

The Lake Albano study area covers 30 km^2. Fig. 1 shows its location in the Lazio Region. The distribution of 149 sub-aerial landslide forms and 65 sub-aqueous forms is in Table 1(a) and Fig. 2, where linear and polygonal forms are grouped into dynamic types in the two physical settings, above and below the water level of the lake shown as a blue line. In the illustration, they overlay an enhanced digital elevation model. The three platforms and the two escarpments are well visible in the model providing the physical context of the sub-

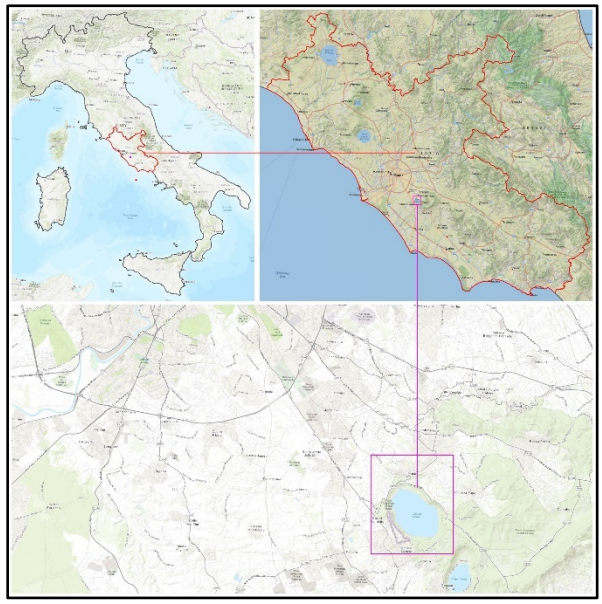

Figure 1: Location of the study area around Lake Albano near Rome, Lazio Region, Italy.

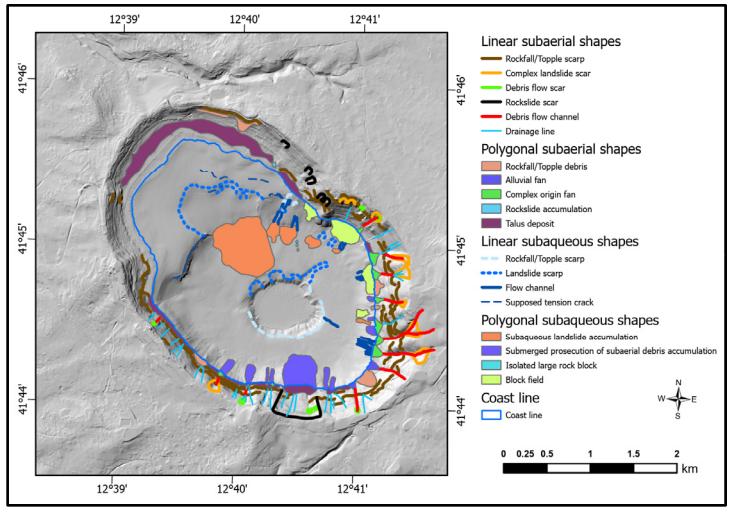

Figure 2: Map distribution of landslide forms of different dynamic types over the internal slopes of Lake Albano in (a), modified after [1].

aqueous forms. A southeast looking 3D view of the lake and its surrounding can be seen in Fig. 3.

The digital images of the individual groups of landslide forms, shown in Fig. 2, were instrumental in representing their distribution within the physical context of other digitized

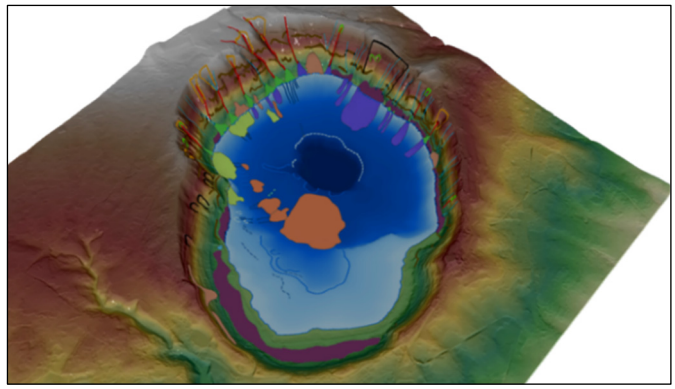

Figure 3: Southeast-looking 3D view of Lake Albano and the landslide forms.

maps: land use, lithology, digital elevation model, and its derivative continuous fields of aspect, slope, curvature, planform, and profile, listed in Table 1(b). Eleven classes of land uses and six lithological units were available from public sources. However, these were heterogeneous, of diverse periods, of different resolutions and poorly compatible with maps of slope failure processes. For those reasons, land use and lithology may not have a sufficient or appropriate resolution not only in spatial terms but also in the type and number of classes or map units. Finer and more focused mappings, although desirable, were not available to date [1].

The abbreviations in column 2 of Table 1(b) were used in various experiments to indicate the inputs in each experiment. Minimum and maximum values, in columns 3 and 4, indicate the numerical ranges of each continuous field. The description of each ISP, in column 5, indicates the implied relationships with the landslide processes.

Table 1: (a) Landslide forms and short names of the Lake Albano study area classified according to Cruden and Varnes [8] and Mulder and Cochonat [9]. They were termed direct supporting patterns (DSP). (b) Digitized categorical land use and lithology maps and DTM-derived continuous field maps with value ranges. They were termed indirect supporting patterns (ISPs).

(a)			
Sub-aerial linear forms		**Sub-aquatic linear forms**	
Debris flow channel	**LT1**	Flow channel	**LA1**
Debris flow scar	**LT2**	Landslide scarp	**LA2**
Drainage line	**LT3**	Rockfall/topple scarp	**LA3**
Rockfall/topple scarp	**LT4**	Supposed tension crack	**LA4**
Complex landslide scar	**LT5**		
Rockslide scar	**LT6**		
Sub-aerial polygonal forms		**Sub-aquatic polygonal forms**	
Alluvial fan	**PT1**	Block field	**PA1**
Complex origin fan	**PT2**	Isolated large rock block	**PA2**
Rockfall/Topple debris	**PT3**	Sub-aqueous landslide accumulation	**PA3**
Rockslide accumulation	**PT4**	Submerged prosecution of sub-aerial	
Talus deposit	**PT5**	accumulation	**PA4**

Table 1: Continued.

(b)				
Pattern	**Short name**	**Minimum value**	**Maximum value**	**Description**
Land use	**U**	1	11	**U_1**, Wooded areas; **U_2**, Mining areas, construction sites, landfills; **U_3**, Urbanized green areas; **U_4**, Permanent crops; **U_5**, Shrubs or herbaceous vegetation cover; **U_6**, Productive settlement; **U_7**, Residential settlement; **U_8**, Stable lawns (permanent forages); **U_9**, Arable land; **U_{10}**, Heterogeneous agricultural areas; **U_{11}**, Open areas with sparse or absent vegetation
Lithology	**L**	1	6	**L_1**, Breccia; **L_2**, Gravel/sand/clay; **L_3**, Silt/clay; **L_4**, Lava (leucititis/trachyte); **L_5**, Slag/lapilli; **L_6**, Tuff
Aspect	**a**	0	359 d	In degrees from the north direction
DTM (elevation)	**d**	121.95 m	636.15 m	In m.a.s.l.
Slope	**s**	0 d	76.04 d	In degrees
Curvature	**c**	−236.58	241.66	Planform + Profile
Planform	**f**	−151.60	149.05	Divergence and convergence of the water flow (+ convex surface; − concave surface in direction of maximum slope)
Profile	**p**	−135.87	117.87	Acceleration and deceleration of the water flow (+ concave surface; − convex surface perpendicularly to the direction of maximum slope)

Fig. 4 shows the database of raster images. They were digitized at a resolution of 5 m × 5 m within a raster of 1002 pixels × 1202 lines (= 1,204,404 pixels), all in pixel-to-pixel correspondence. Within such raster, 975,093 pixels occupy the sub-aerial (terrestrial) part of the study area, while 229,311 pixels correspond to the sub-aqueous part.

In our analysis, the images of the presence of landslide forms were considered as direct supporting pattern, DSP, for the modelling. The remaining images were considered as indirect supporting patterns, ISPs, hopefully representing the typical setting of the landslides. Patera and Fabbri [1] constructed and discussed the database and its properties.

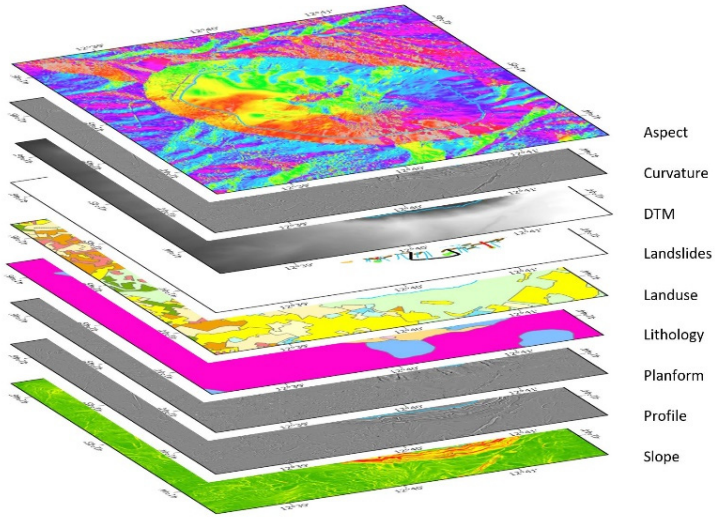

Figure 4: The database of digital images used for landslide susceptibility modelling in the Lake Albano study area, modified after [1].

Mathematical models of spatial prediction are to establish spatial relationships between DSP and ISPs and integrate them into *prediction patterns* representing the likelihood of future occurrences. For this, a unified mathematical framework and appropriate strategies are required. Chung and Fabbri [10] termed it "favourability function" modelling. Favourability modelling was applied to the database of Lake Albano. Following are terminology and strategies for the corresponding approach.

3 FAVOURABILITY FUNCTION MODELLING

The term "favourability" was proposed [10] to allow constructing functions for modelling the prediction of spatial patterns of future events given information on past events and their physical and possibly temporal settings. The mathematical framework of favourability function modelling is intended for applications in the fields of resource exploration and of natural hazard/risk assessment among others.

The applications could be made using different interpretations of the spatial relationships observed in areas where the hazardous events occurred (or resources discoveries were made). In essence, a favourability function is based on a proposition, i.e. a mathematical statement, to be proven true given the evidence available in the study area.

Because in our case we are dealing with landslides occurrences, representing the hazardous events, a modelling proposition is the following:

$$\mathbf{P}_i\text{: that a point } \boldsymbol{i} \text{ in the study area is affected by a specific type of occurrence} \mid \text{the presence of spatial evidence,} \quad (1)$$

where the symbol $\mid$ indicates "given", the point $\boldsymbol{i}$ is a pixel of 5 m resolution, the specific type of occurrence is the presence of one of the landslide forms in Fig. 2 (the DSP), and the spatial evidence is the presence of one or more of the classes, units or values in the images in Fig. 4 (the ISPs).

To support the proposition in (1) we can explore the database, constructed by experts for the study area, and establish spatial relationships between the spatial evidence at the locations of the occurrences, DSP, and that at the locations of their absence. Obviously, we expect the study area to be suitable to provide the support sought, and the setting in the presence of the landslides to differ from that in their absence.

A common way to establish the spatial relationships between the presence and the absence in a study area is to calculate the empirical likelihood ratios or ELR. It consists of obtaining first the normalized frequencies of the DSP, the area proportion occupied by a given type of landslides, within the study area for each ISP. Some ISPs are the categorical maps partially representing their setting, e.g., land use and lithology for the sub-aerial forms. In addition, we calculate the corresponding density functions for the presence of the ISPs of continuous fields, e.g. aspect, DTM, slope, etc. We do the same also for the areas in which we assume the absence of the forms in the remainder of the study area. The ratio of the two normalized frequencies or density functions is the ELR, whose values range from zero to infinity. For instance, if for a pixel ELR is 2, it means that the frequency in the presence of the landslides is twice that in their absence in the study area. Should the ELR be equal to 1 it means that the two frequencies are the same in the presence of the landslides or in their absence in the study area. We tentatively interpret that ELR values ≥ 2.00 are supporting the modelling while values $\cong 1$ are not in support.

Establishing such spatial relationships is a first step in spatial modelling. There are many mathematical models for the integration of spatial relationships in favourability modelling, e.g. to measure the sureness or probability or certainty or belief, plausibility or possibility that the proposition in (1) is true. Chung and Fabbri [10] discussed Probabilistic, Certainty Factors, Dempster–Shafer Belief Function, and Fuzzy Logic Membership functions. Each interpretation and mathematical model requires a number of different assumptions.

Other assumptions are necessary concerning the database, the spatial relationships of DSP and the ISPs, and the strategy of processing. Fabbri and Chung [11] and Fabbri and Patera [12] discuss some of the assumptions in modelling landslide hazards. These are not going to be introduced here but mention will be made in the application examples. As a general procedure of predictive modelling we have selected the following steps:

1. Compute the spatial relationships and integrate them by a mathematical model;
2. Generate a prediction image from the integration and obtain from it a *prediction pattern* by sorting the values in descending order and equal-area ranking;
3. Cross-validate the *prediction pattern* to evaluate the quality of the prediction and generate prediction-rate curves for interpretation;
4. Estimate the uncertainty associated with the *prediction pattern* using a model and compare it to the uncertainty associated with patterns from different mathematical models.

In the applications that follow, we present the results of steps 1 to 3 and provide some anticipation of what to expect from a step 4. The two mathematical models applied are the Fuzzy Set function [10], [13], short named **FZ**, and the Logistic Regression Function [14], [15], short named **LO**.

4 EXAMPLE OF LANDSLIDE PREDICTION PATTERNS

The application example indicates how well we can answer the question in the title of this contribution. The procedure consists of the four steps introduced above. Spatial-relationship tables, *prediction patterns*, prediction-rate curves and overlays of top ranks are the modelling results for interpretation. To guide through steps and experiments, various short names

indicate in sequence: the mathematical models, the direct supporting pattern, number of individual landslide occurrences and the sequence of indirect supporting patterns used in the analysis. The results of predictive modelling are the *prediction patterns*, i.e. all the pixels whose values are the possibility of future occurrences: for instance, the result of a Fuzzy Set function modelling for debris flow channel susceptibility in Table 1 is **FZ_LT1_9_ULads**.

4.1 The ELR tables

ELR values provide a relative measure of support for the modelling, i.e. for the proposition in (1). The DSP is the set of pixels with the presence of the landslides in the study area and the ELR values are a measure of contrast between the setting in the presence of the landslides and that in their absence in the study area.

Table 2 shows the sub-aerial landslide form names and short names in column 1, the number of individual landslides in column 2 and the corresponding number of pixels affected in column 3. Column 4 lists the ELR values for categorical ISPs. Column 5 shows the ELR values for continuous field ISPs. For the latter, the range of values above a threshold of ≥ 2 (sometime ≥ 1) are in italics font and within brackets is the maximum ELR reached and its corresponding value. All ELR values ≥ 2.00 are in bold fonts in the table. This simplification synthesizes histograms for categorical ISPs and functions for continuous-field ISPs for each landslide form.

For the polygonal forms, the number of pixels refers to the higher parts of approximately 15% of the area that represent the trigger zones. The terrestrial or sub-aerial part of the study area, visible in Fig. 2, covers 975,093 pixels.

Table 3 shows the ELR values for the sub-aqueous forms. No land use or lithology is available in this case but only the continuous field ISPs. The sub-aqueous part of the study area occupies 229,311 pixels. Here too the ELR values ≥ 2.00 are in bold fonts.

For instance, in Table 2, the first form **LT1**, with 9 debris flow channels affecting 807 pixels, have ratios ≥ 2 for $\mathbf{U_9}$ and $\mathbf{L_1}$, **3.38** and **2.46**, respectively arable land and lava. Supporting ISPs are also **d**, DTM, with values between *453* and *575* m.a.s.l. with a maximum ratio of **6.79** at *541* m elevation; and **s**, slope, between *19* and *72* degrees with a maximum of **7.34** at *56* degrees.

For sub-aerial forms, 120 linear and 29 polygonal in Table 2, we can see that $\mathbf{U_9}$ and $\mathbf{L_4}$ have high ratios for all except **PT5**; $\mathbf{L_1}$ is supportive of **LT5**, **LT6**, **PT3**, **PT4** and **PT5**; $\mathbf{U_{10}}$ is supporting **LT3** and **LT6**. Such common high ratios indicate some similarity of setting of the different landslide forms.

The sub-aqueous forms in Table 3 show groups of landslides with high ratios for distinct elevations: *155* m (**LA2**, **LA3**), *178* m (**PA2**), *200* m (**LA1**), *217* m (**PA3**), *245–246* m (**LA4**, **PA4**) and *282* m (**PA1**); shallow slope angles *4–21* d and *8–9* d (**PA2**, **PA3**), *10* and *20* d (**LA2, LA1**). Except for **LA1** and **PA3**, all other forms have high ELR values for **c**, **f** and **p**. In particular, **PA4** shows wide ranges for **a** and **s**, aspect and slope, *99* and *42* degrees, respectively.

In essence, the tables providing ELR values for each landslide form describe the spatial signature of the landslides within the study area's sub-aerial and sub-aqueous parts. This is what the database can provide the mathematical models for prediction.

Necessary assumptions for the modelling are: that the database sufficiently represents the characteristics of the landslide process, that the ISPs provide factors related to it, that the distribution of the landslides is a sample of a larger population in space and in time, and that we can separate them into two groups, one for modelling and the other for verification being

Table 2: ELR values for linear, **LT**, and polygonal, **PT**, top 15% sub-aerial (terrestrial) forms, DSP, using as ISPs land use, **U**, lithology, **L**, and the continuous fields derived from the elevation, **a**, **d**, **s**, **c**, **f** and **p**. Abbreviations are as in Table 1. Values are bold if ELR ≥ 2.00. The corresponding ranges of classes are in italics with the maximum class and ratio in brackets.

Sub-aerial linear forms				
Forms	**No.**	**Pixels**	**Categorical ISP**	**Continuous ISP**
LT1 Debris flow channel	9	807	**U_9=3.38**; U_{10}=1.92; L_1=1.05; **L_4=2.46**; L_6=0.78	a ≥ 1 *145–211* (max 1.94 at *171*d), *245–330* (max 1.42 at *307*d); **d** ≥2 *453–575* (max **6.79** at *541*m); **s**≥2 *19–72* (max **7.34** at *56*d)
LT2 Debris flow scar	14	764	**U_9=3.76**; U_{10}=1.07; **L_1=2.26**; **L_4=2.44**; L_5=1.73; L_6=0.34	a ≥ 1 *177–244* (max 1.55 at *206*d), *285–337* (max 1.34 at *309*d); **d** ≥2 *479–496* (max **2.03** at *487*m); *528–569* (max **2.65** at *551*m); **s** ≥2 *22–70* (max **12.92** at *57*d)
LT3 Drainage line	7	177	**U_9=3.22**; **U_{10}=3.29;** L_1=1.41; L_4=1.64; L_6=0.91	**a** ≥2 *0–83* (max **3.76** at *14*d); *353–361* (max **2.30** at *361*d); **d** ≥2 *430–519* (max **4.54** at *469*m); **s** ≥2 *22–73* (max **82.39** at *73*d)
LT4 Rockfall topple scarp	33	1344	**U_9=4.01**; **L_1=10.72**; L_2= 0.18; **L_4=2.60**; **L_5=2.84**; L_6=0.23	**a** ≥2 *0–75* (max **3.89** at *16*d); **d** ≥1 *334–503* (max 1.95 at *449*m); **s** ≥2 *23–72* (max **11.50** at *46*d)
LT5 Complex landslide scar	51	2969	**U_6**=0.18; **U_9=3.44**; U_{10}=1.93; **L_1=9.15**; L_2=0.35; **L_4=3.29**; **L_5=6.40**; L_6=0.16	**a** ≥2 *25–84* (max **2.88** at *53*d); **d** ≥1 *305–414* (max 1.80 at *354*m); *426–484* (max 1.52 at *459*m); **s** ≥2 *25–75* (max **67.90** at *72*d)
LT6 Rockslide scar	6	500	U_1=0.19; **U_9=2.09**; **U_{10}=7.15;** **L_1=3.90**; **L_4=3.36**; L_6=0.46	**a** ≥2 *0–45* (max **2.70** at *29*d); **d** ≥2 *386–415* (max **2.21** at *400*m); *479–524* (max **3.86** at *502*m); **s** ≥2 *22–66* (max **9.79** at *38*d and max **4.69** at *60*d)

Table 2: Continued.

Sub-aerial polygonal forms				
Forms	**No.**	**Pixels**	**Categorical ISP**	**Continuous ISP**
PT1 Alluvial fan	2	95	**U_9=4.01**; **L_4=6.91**	**a** ≥2 *309–352* (max **3.09** at *351*d); **d** ≥2 *294–345* (max **4.90** at *320*m); **s** ≥2 *18–37* (max **8.20** at *24*d)
PT2 Complex origin fan	11	416	**U_9=3.81**; U_{10}=0.84; **L_1=2.04**; **L_2=16.83**; **L_4=3.72**; **L_5=6.38**	**a** ≥2 *262–298* (max **2.54** at *280*d); **d** ≥2 *292–345* (max **4.48** at *320*m); **s** ≥2 *20–68* (max **7.20** at *42*d)
PT3 Rockfall topple debris	6	543	**U_9=3.94**; U_{10}=0.31; **L_1=3.13**; **L_2=2.44**; **L_4=3.32**; L_6=0.44	**a** ≥2 *49–65* (max **2.30** at*57*d); *184–210* (max **2.60** at *196*d); **d** ≥2 *324–378* (max **2.72** at *350*m); **s** ≥2 *20–69* (max **7.85** at *34*d, max **8.25** at *62*d)
PT4 Rockslide accumulation	1	14	**U_6=2.42**; **U_9=2.29**; **L_1=24.99**	**a** ≥2 *200–249* (max **4.58** at *221*d); **d** ≥2 *274–328* (max **5.07** at *302*m); **s** ≥2 *14–27* (max **9.66** at *20*d)
PT5 Talus deposit	9	1883	U_1=0.48; U_6=1.13; **U_8=2.85**; U_9=1.46; U_{10}=1.06; **L_1=23.69**; L_2=0.70; L_4=0.34; **L_5=4.60**	**a** ≥2 *174–227* (max **3.71** at *198*d); **d** ≥2 *284–338* (max **4.75** at *313*m); **s** ≥1 *35–70* (max1 **4.56** at *51*d and max2 **7.98** at *69*d)

the two groups of comparable nature. In addition, the assumption made in generating the ELR values is that the part of the study area without landslide occurrences (or in which occurrences are unknown) shows sufficient contrast of signature for the modelling.

4.2 **FZ** and **LO** prediction patterns

The ELR values are the support that the database provides to the modelling. A *prediction pattern* is the result of applying a mathematical model for normalizing and integrating the ELR values into a relative favourability index to classify the study area, i.e. the prediction rates.

The *prediction patterns* of sub-aerial landslides in Fig. 5 were obtained applying the two models of Fuzzy Set function, **FZ** [13] (gamma function operator with $\gamma = 0.5$), and Logistic Discriminant function, **LO** [15]. The prediction rates of a model are the results of normalization and combination rules that differ from model to model. So that the resulting prediction image has values between a minimum and a maximum, not interpretable as such.

Table 3: ELR values for linear, **LA**, and polygonal, **PA**, higher 15% sub-aqueous forms, DSP, using as ISPs the continuous fields derived from the elevation, **a**, **d**, **s**, **c**, **f** and **p**. Abbreviations are as in Table 1. Values are bold if ELR ≥ 2.00. The corresponding ranges of classes are in italics with the maximum class and ratio in brackets.

Sub-aqueous linear forms			
Forms	**No.**	**Pixels**	**Continuous ISP**
LA1 Flow channel	21	578	**a** ≥ 2, *242–313* (max **5.03** at *285*d); c ≥ 1 *−43* to *−3* (max 1.14 at *−34*); **d** ≥ 2, *205–234* (max **2.39** at *217*m); f ≥ 1 *−26* to *−2* (max 1.15 at *−20*); p ≥ 1 *2–34* (max 1.48 at *28*); **s** ≥ 2, *0–76* (max **4.04** at *20*d)
LA2 Landslide scarp	10	1154	**a** ≥ 2, *154–183* (max **2.10** at *162*d); **c** ≥ 2, *215–222* (max **2.40** at 218); **d** ≥ 2, *146–166* (max **4.58** at *155*m); *238–261* (max **4.14** at *251*m); f ≥ 1, *139–150* (max 1.99 at *142*), *156–168* (max 1.50 at *162*); **p** ≥ 2, *148–153* (max **2.43** at *151*); s ≥ 1, *6–26* (max 1.92 at *10*d)
LA3 Rockfall/ topple scarp	5	444	**a** ≥ 2, *0–90* (max **2.23** at *0*d); **c** ≥ 2, *218–220* (max **2.03** at *219*); *254–274* (max **6.86** at *265*); **d** ≥ 2, *144–173* (max **10.08** at *155*); **f** ≥ 2, *135–144* (max **4.61** at *138*), *159–166* (max **3.46** at *163*); **p** ≥ 2, *113–128* (max **9.36** at *120*); **s** ≥ 2, *12–20* (max **2.95** at *16*d), *27–36* (max **3.04** at *32*d)
LA4 Supposed tension crack	6	456	**a** ≥ 2, *109–116* (max **2.03** at *112*d); *139–197* (max **3.51** at *166*d); **c** ≥ 2, *260–270* (max **2.16** at *266*); **d** ≥ 2, *230–268* (max **7.31** at *245*m); **f** ≥ 2, *164–165*; (max **2.03** at *165*); **p** ≥ 2, *118–125* (max **2.75** at *121*); **s** ≥ 2, *26–39* (max **6.68** at *33*d)
Sub-aqueous polygonal forms			
PA1 Block field	4	696	**a** ≥2 *194–285* (max **3.91** at *260*d); **c** ≥2 *−91* to *−16* (max **103.46** at *−47*); *+41* to *+80* (max **6.19** at *+66*); **d** ≥2 *267–290* (max **7.03** at *282*m); **f** ≥2 *−38* to *−8* (max **187.19** at *−38*); *+7* to *+20* (max **8.99** at *+13*); **p** ≥2 *−35* to *−19* (max **6.01** at *−29*); *+9* to *+50* (max **84.05** at *−26*); **s** ≥2 *26–63* (max **104.54** at *52*d)
PA2 Isolated rock block	3	21	**a** ≥2 *112–173* (max **4.23** at *144*d); c ≥1 *0* to *+18* (max 1.26 at *+13*); **d** ≥2 *168–188* (max **3.72** at *178*m); f ≥1 *0* to *+9* (max 1.35 at *+8*); p ≥ 1 *−11* to *+1* (max 1.08 at *−7*); **s** ≥2 *4–21* (max **2.10** at *4*d)
PA3 Sub-aqueous landslide accumulated	6	1231	**a** ≥2 *10–14* (max **2.65** at *12*d); c ≥1 *−1* to *+20* (max 1.12 at *+15*); **d** ≥2 *184–211* (max **5.34** at *200*m); f ≥1 *0* to *+10* (max 1.15 at *+7*); p ≥1 *−11* to *0* (max 1.07 at *−8*); **s** ≥2 *8–9* (max **2.05** at *9*d)
PA4 Submerged prosecution of sub-aerial accumulation	10	3461	**a** ≥2 *0–49* (max **4.85** at *0*d), *310–360* (max **7.16** at *360*d); **c** ≥2 *−75* to *−46* (max **2.57** at *−56*); **d** ≥2 *230–290* (max **2.84** at *246*m); **f** ≥2 *−45* to *−30* (max **2.86** at *−38*); **p** ≥2 *+25* to *+45* (max **4.47** at *+36*); **s** ≥2 *17–57* (max1 **4.60** at *25*d, max2 **6.15** at *42*d)

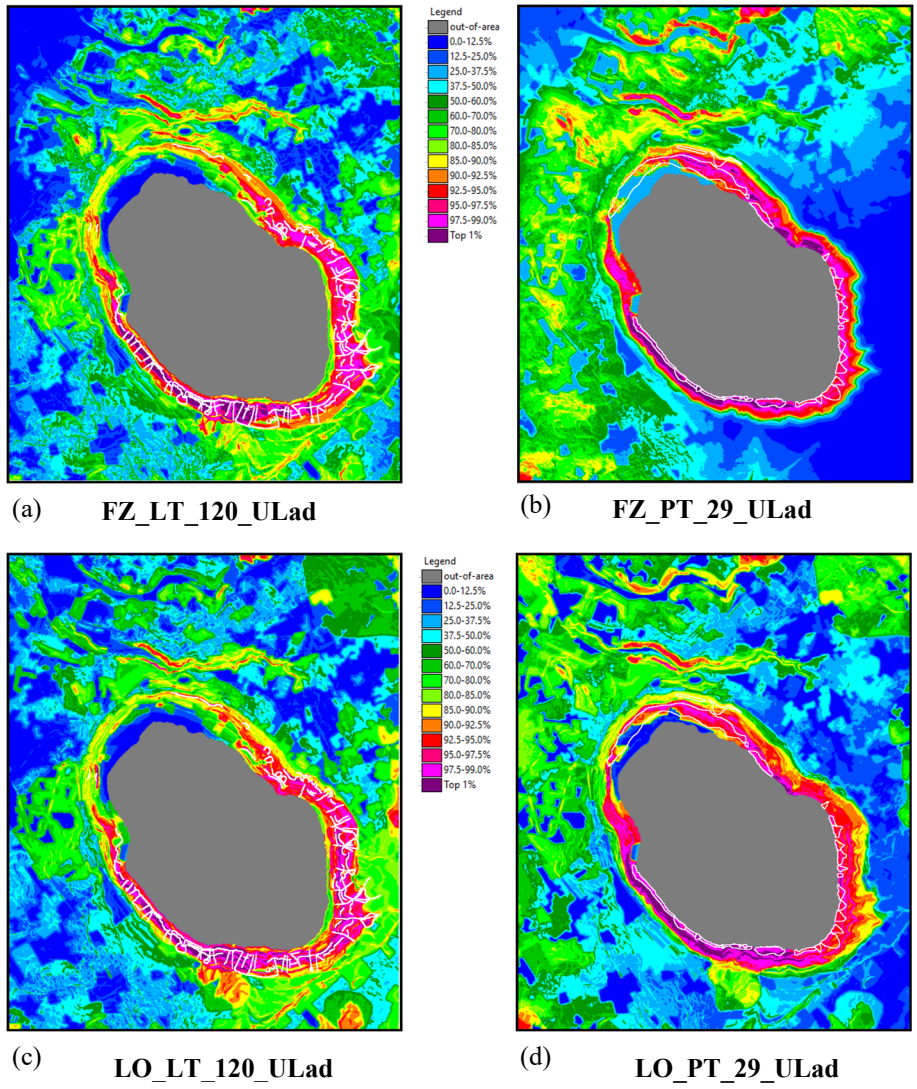

Figure 5: **FZ** (a) and (b), and **LO** (c) and (d) prediction patterns for linear and polygonal sub-aerial landslides, **LT_120** and **PT_29**, respectively.

By sorting these values in decreasing order and converting them into equal-area ranks we can visualize and interpret them as *prediction patterns*, i.e. spatial configurations of classes of recognizable shapes and locations.

In our case, we generated 200 equal-area ranks, each corresponding to 0.5% of the study area of 975,093 pixels, i.e. 4875 pixels. The ranks were then grouped into wider classes for the lower values and narrower classes for increasingly higher values of greater concern. Each class was then assigned a color from a pseudo-color look-up table according to the legend of the patterns. The legend was maintained the same for all patterns to allow recognition and comparison.

In the four illustrations of Fig. 5, the contours of the landslides used for modelling are superimposed as white lines. The classes from orange to purple, the top 10% of the study area, indicate the areas with the highest susceptibility to linear and polygonal sub-aerial landslide occurrences. In particular, the top 1% ranks, purple, indicate the critical areas and differences between patterns, useful for comparing **FZ** and **LO** predictions for either **LT** or **PT** landslides. There are similarities and differences to consider around the lake.

The density of the 120 **LT** landslides is high and the predicted areas of susceptibility concern are the ones far from the landslide occurrences in white in the patterns of Fig. 5. We can observe that the top 1% ranks are distributed along the southwestern coastline in Fig. 5(a) but in Fig. 5(c) they extend to the eastern part. Comparing the patterns in Fig. 5, we can see that the top 1% ranks extend to the northeastern parts in Fig. 5(b) while they are mostly on the southwestern coast in Fig. 5(d). The southwestern concentration of higher ranks indicates high susceptibility for both the linear and the polygonal sub-aerial landslides.

Assumptions combining the support of ISPs are of conditional independence of categorical, continuous fields and of their aggregation. Generally, in the earth science, maps are frequently conditionally dependent, and such dependence has to be verified to make sure it is not affecting the *prediction patterns*.

Furthermore, we need to know: how "good" the patterns are as predictors of "future" landslides of the same broad group of forms, linear or polygonal? This we attempt in the next section through cross-validation strategies.

4.3 Prediction-rate curves from cross-validations

Ideally, a prediction uses past and present event data to predict future events. However, we do not have sufficient information on the time of occurrence of the landslides in the Lake Albano area. What we can do is to partition a set of landslides into a modelling group and a cross-validation group, pretending that this second group represents the future landslide occurrences.

Cross-validation is the process of generating a *prediction pattern* using the modelling set and verifying the predicted values in the locations of the cross-validation set. The process can be iterative as sequential exclusion of a selected number of occurrences, as sequential selection, or as random selection repeated a convenient number of times [16].

Prediction-rate curves show on the horizontal axis the cumulative proportion of study area classified as susceptible, with ranks in decreasing order. On the vertical axis, they show the corresponding cumulative proportion of cross-validation occurrences.

In Fig. 6(a) and 6(b), the solid black curves are the results of iterative processes **FZ_LT_120m8_ULads** and **FZ_PT_29m2_Ulads**, where **m** indicates minus for exclusion of **8** and **2** occurrences. The curves are obtained by integrating the results of 15 and 14 iterations, respectively. The varicolored thinner curves are from the individual iterations where **8** or **2** occurrences were considered as the "next" ones.

The iterations in Fig. 6(a) show limited variability of curves that are all very steep and represent extremely good predictions. The top 5% ranks predict 60% of the occurrences and the top 10%, 87%, and top 15%, 99% on the thick black curve. In Fig. 6(b), the thick black curve shows a lower variability up to the top 5%. The top 5% predicts 45%, the top 10%, 53% and the top 15%, 58% of the occurrences. It is with iterations 9th and 13th that high deviations appear, i.e. lower prediction rates for the two corresponding pairs of landslides. Note the similarity of the solid red and blue curves in Fig. 6(c) with the solid black ones in Fig. 6(a) and 6(b). It means that the two models, **FZ** and **LO**, generate rather similar

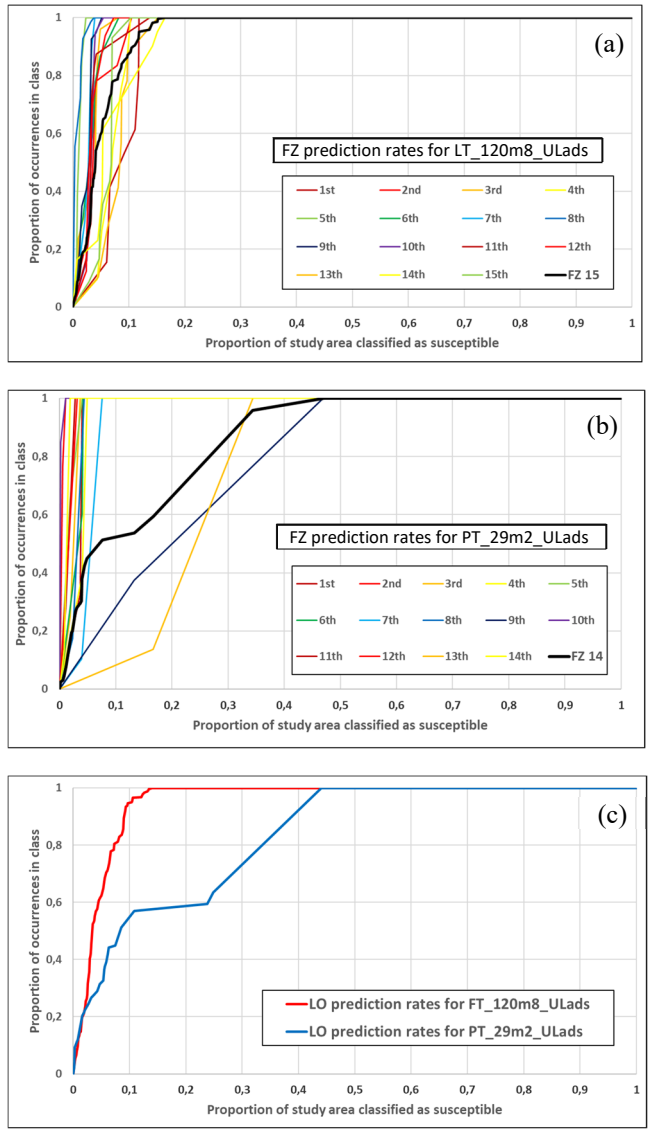

Figure 6: Prediction rate curves for the prediction patterns of linear and polygonal forms in Fig. 5. (a) The curves from iterative procedure **FZ_LT_120m8_ULads**; (b) The curves from **FZ_PT_29m2_ULads**; and (c) The curves from procedures **LO_LT_120m8_ULads** and **LO_PT_29m2_ULads**.

predictions. Altogether, having such limited variability in the prediction-rate curves means that the prediction patterns show low uncertainty of ranking.

Assumptions in the cross-validation process are that we can separate the landslides into two or more sets, younger and older to verify the consistency of *prediction patterns*, that we can assess the uncertainty associated with the patterns. To perform step 4, mentioned in Section 3, because the iterative cross-validation generated a prediction pattern per iteration,

the set of patterns can be used for statistical analyses estimating the relative uncertainty associated with the initial pattern [12]. In our case the prediction-rate curves signal already a limited uncertainty

What are the significant parts of the prediction-rate curves and the corresponding top ranks in the *prediction patterns*? Can we compare the patterns for sub-aerial linear landslides with the polygonal ones? Can we compare the patterns with **FZ** models with those with **LO** models? This is done in the next section.

4.4 Comparison of top ranks of patterns

To visualize and interpret the degree of similarity of *prediction patterns*, a simple procedure was followed. The top 5% ranks from patterns **FZ_LT_120_ULads** and **FZ_PT_29_Ulads** were converted to numerical values of 1 while the remainder of the study area was converted to 0. Here we assume, tentatively, that the meaningful (or convenient) part of the prediction patterns is the top 5% ranks.

The corresponding binary, 0-1 images were overlaid with an operation of crossing to obtain a table of paired values, 0*0, 0*1, 1*0, and 1*1 with associated numbers of pixels, and a crossing image as shown in Fig. 7(a). The same procedure was applied to obtain Fig. 7(b) for the crossing of **FZ_LT_120_ULads** and **LO_LT_120_ULads**.

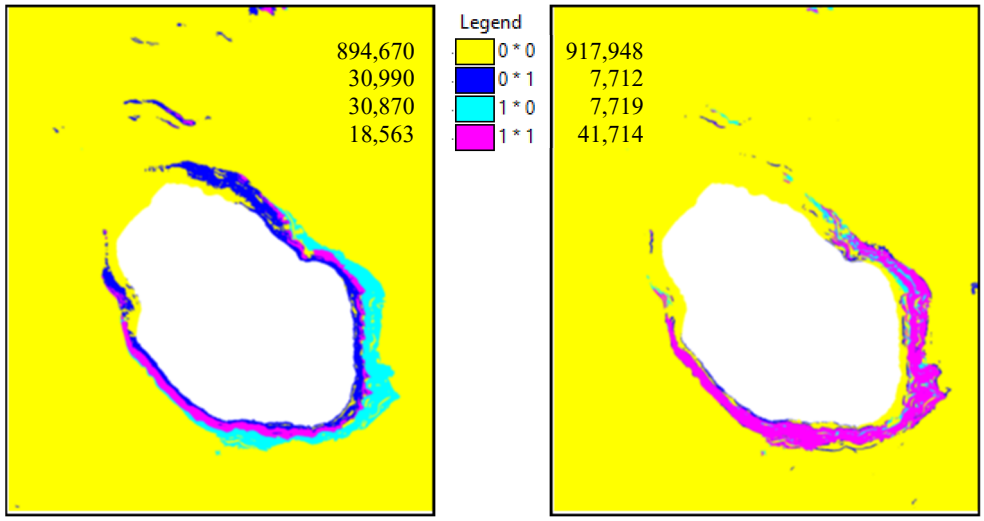

(a) **FZ_LT_120_ULads**
FZ_PT_29_ULads

(b) **FZ_LT_120_ULads**
LO_LT_120_ULads

Figure 7: Overlaps of the top 5% ranks of **FZ** and **LO** prediction patterns. (a) Overlaps of prediction patterns for **FZ** linear and polygonal forms; and (b) Overlaps of **FZ** and **LO** *prediction patterns* of linear forms. Legend indicates the number of overlapping top 5% ranking pixels.

The wide overlap, 1*1, of Fig. 7(b) shows that the corresponding *prediction patterns* are very similar and robust to changes in mathematical models. The limited overlap, 1*1, of Fig. 7(a), on the contrary, shows a limited but consistent overlap, 1*1, of higher susceptibility

ranks for linear and/or polygonal sub-aerial landslides. They confirm the co-occurrence of susceptibilities to the different landslide forms, linear and polygonal.

Let us now consider a form of polygonal sub-aqueous landslides like Submerged prosecution of sub-aerial accumulation and generate *prediction patterns* in the sub-aqueous part of the study area, using the same two mathematical models.

4.5 Prediction of a polygonal sub-aqueous form

The sub-aerial forms **LT** and **PT** appear robust to changes in the mathematical model, from **FZ** to **LO**. In most cases in different studies the same robustness has been observed [11], [17]. However, for polygonal sub-aqueous form **PA4**, see the bottom of Table 3 for the ELR values, we observed a sensitivity to the models.

PA4 consists of 10 landslides, of which we later used their higher 15% pixels as DSP. We could only use **ads cfp** as ISPs and the sub-aqueous study area of 229,311 pixels. As can be observed in Table 3, all the 6 ISPs generate high ELR values, therefore all being supportive of the proposition in (1). The *prediction patterns* in Figs 8(a) and 7(b), **FZ_PA4_10_ads_cfp** and **LO_PA4_10_ads_cfp** show sharp differences. This in spite of the prediction rate curves from cross-validations processes (**FZ_PA4_10m1_ads_cfp** and **LO_PA4_10m1_ads_cfp**) generating very steep prediction-rate curves in Fig. 8(c). The top 5%, 10% and 15% ranks predict 50%, 95% and 100% of the occurrences for **LZ**, and 50%, 79% and 99% for **LO**. Fig. 8(d) shows the overlaps of their top 5% ranks (11,476 pixels) where 1*1 consists of 4,613 pixels while 0*1 and 1*0, consist of 7,000 and 6,976 pixels, respectively. In the illustration, the borders of the polygonal landslides have been plotted in black.

Observing the ELR values at the bottom of Table 3, we can say that aspect, **a**, and slope, **s**, have bimodal ELR functions that are given more weight by the **LO** model with extension of the top 5% ranks in the northeastern direction of the coastline. In both the models, the support of ISPs **c**, **f** and **p** is redundant. Prediction made without them appears identical to the ones using them being they highly correlated with elevation. While more can be done with the remaining sub-aqueous forms, analyzing the **PA4** landslides is a first step after the study of the sub-aerial ones.

5 CONSIDERATIONS AND CONCLUDING REMARKS

What are the limitations, complexities and improvements of the study and database?

Our analysis of the Lake Albano database have so far provided a clear answer to the question title of this contribution: Can we assess landslide hazard in the volcanic crater of Lake Albano? In reality, we had to deal with susceptibility because the times of occurrence of the landslides are not available.

The ELR tables provide clear support to favourability function modelling so that the *prediction patterns* of both the linear and the polygonal sub-aerial landslides are reliable representations of where future occurrences are to be expected. The sub-aerial patterns, given the similarities of settings and the high density of occurrences, had to be generated by grouping them into 120 linear and 29 polygonal landslides. The corresponding aggregated prediction-rate curves are very steep, “good predictions”, and show very limited variability, which translates into low uncertainty of ranking.

For this reason, we have arbitrarily selected the top 5% ranks of the *prediction patterns* (48,750 pixels or ≅1.22 km^2 in the sub-aerial part of the study area) as the areas of relatively high susceptibility. Their overlaps from two different models, **FZ** and **LO**, and from the two groups of linear and polygonal landslides, show high degrees of similarities and robustness.

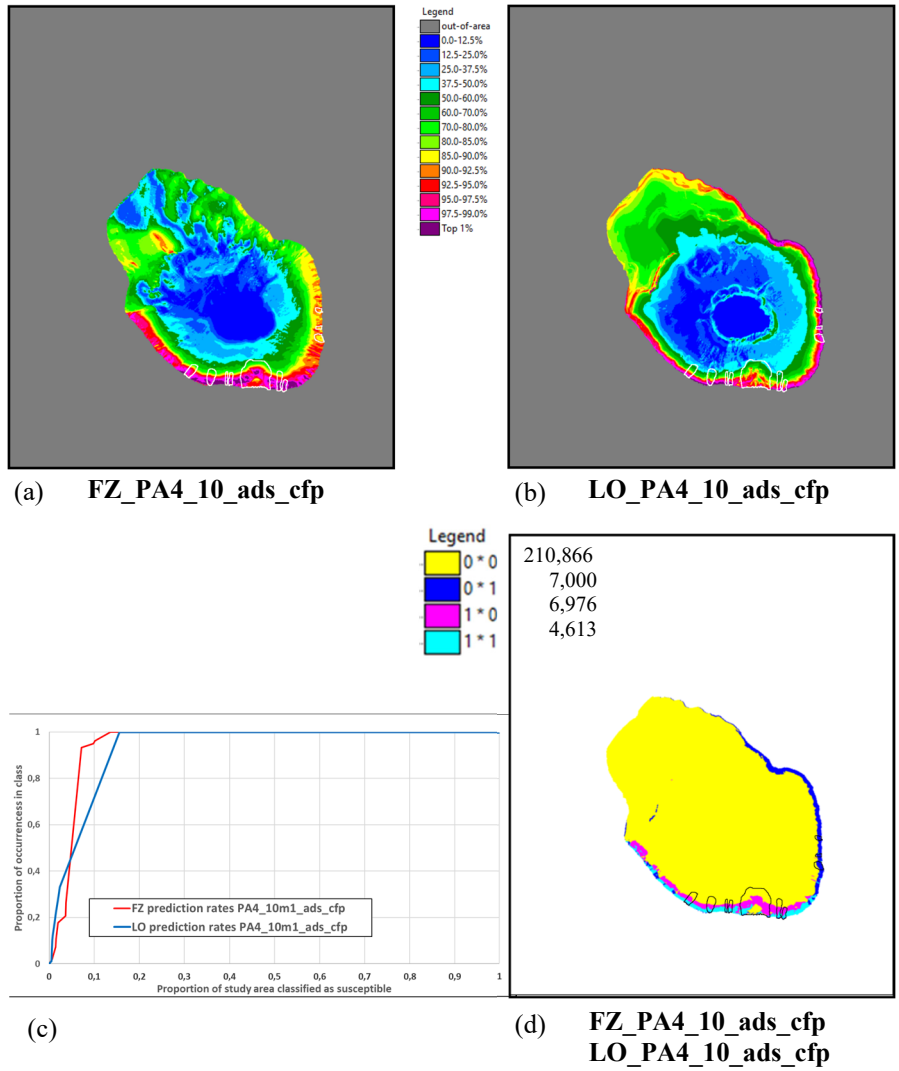

Figure 8: **FZ** and **LO** (a) and (b) prediction patterns for polygonal sub-aqueous landslides, FP4_10, contours in white. In (c) the corresponding 10m1 prediction-rate curves. In (d) the overlaps of the corresponding top 5% ranks of the two patterns, contours in black.

One example of prediction patterns from sub-aqueous polygonal landslides, while describing a particular setting of prosecution of sub-aerial accumulations, provides a particular instance of sensitivity to the two models due to wide spatial relationships of aspect and slope angles.

The following points are worth considering.

(i) Prediction of landslide susceptibility is very good: we know where the next sub-aerial occurrences will show up;

(ii) Anticipating the occurrences is good but the evidence is very wide: one should, in the future, use more appropriate and detailed land use and lithology maps;
(iii) Measures of mitigation of hazard or risk avoidance can be taken or applied with confidence over the patterns;
(iv) Much activity is taking place for protecting the Lake Albano's environment through a multitude of initiatives as documented in the Appendix;
(v) How could we interpret or estimate the likelihood that local administrations and communities are willing to invest in prevention, i.e. before the next disasters occur?
(vi) Could a more holistic approach consider additional multiple hazards such as volcanism, seismicity, and hydrologic conditions in the area?
(vii) Who could use the results of the assessments? Civil protection agencies, local authorities, public associations for the protection of the lake?
(viii) What is the societal convenience of acting in consequence of the assessment? Who benefits from the safeguard actions undertaken?

We can see that the question, title of this contribution, is loaded with incredulity and uncertainty, not on the technical feasibility of the task of obtaining reliable *prediction patterns* but on estimating the willingness to accept evaluations in order to manage such hazards and consequent risks of "future" events.

APPENDIX

Cultural activities

Compagnia dei viandanti https://compagniadeiviandanti.com/standby/anello-del-lago-di-albano/ Excursion to discover Lake Albano and its peculiarities.
Carpfishing Castelli Romani https://www.facebook.com/Carpfishing-Castelli-Romani-170702572974269/ Sport, fishing.
Federcanoa https://www.federcanoa.it/home/news/27-fick-news/5238-laghi-sicuri-il-centro-federale-di-castel-gandolfo-base-operativa-per-il-soccorso-in-acqua.html Canoe Kayak Italian Federation.
Canoa Kayak Academy https://www.ckacademy.it/ Canoa Kayak Academy.
Associazione Italiana per la lotta alle Sindromi Atassiche https://www.aisasport.it/ Canoe Sport Activities.
Latium Volcano Associazione Ecologica Ambientale https://www.latiumvolcano.it/passeggiateculturali_castelliromani.html Historical, cultural and artistic itineraries in the Castelli Romani.

Groups and associations for the protection of Lake Albano

Facebook public group: *Salviamo il Lago Albano!!!* https://www.facebook.com/groups/salviamoillagoalbano/ Most active Facebook group that offers initiatives, meetings, and proposals.

Associazione Castel Gandolfo in Movimento https://castelgandolfoinmovimento.blogspot.com/2019/07/lago-albano-di-castel-castel-gandolfo.html The purpose of the association is to raise public awareness of safety, legality, cleanliness, and respect for the public beach.
Parco dei Castelli Romani: ***Associazione Bernacca Onlus*** https://www.parcocastelliromani.it/inners/pages/webcam-sul-lago-albano The *Bernacca* non-profit association has activated a panoramic webcam on Lake Albano, in the municipality of Castel Gandolfo, in the Castelli Romani Regional Park.
Meteocastelli http://www.meteocastelli.it/stazioni-meteo/stazione-meteo-del-lago-albano-e-di-castelgandolfo Weather, webcam and geophysics services from Castelli Romani – Colli Albani: Weather station of Lake Albano
RESEDA S.c.s.i. http://www.resedaweb.org/salvaguai/index.htm RESEDA is a non-profit cooperative society that operates in the field of ecology, renewable energy sources, defense of the environment and for the integration of disabled people.
Associazione Amici del Parco dei Castelli Romani https://www.amiciparcocastelliromani.it/ita-chi-siamo Friends of the Castelli Romani Park Association is as an association with a naturalistic, sporting and cultural character, pursuing non-profit and social solidarity purposes.
Arco di Diana APS: ***Gruppo di Studi ricerca archeologica*** http://www.arcodidiana.com/ The association manages the site that hosted the Roman port on the shores of Lake Albano.
Italia Nostra: ***Sezione Castelli Romani*** https://www.italianostra.org/sezioni-e-consigli-regionali/lazio/castelli-romani/ The association is active in the field of the water crisis that has hit Lake Albano in the last 30 years, due to both the consumption of the soil and the increasing of resident population.
CIRF – Centro Italiano per la Riqualificazione Fluviale: ***Webinar SOS Laghi Albano e di Nemi*** https://www.cirf.org/it/webinar-sos-laghi-albano-e-di-nemi/ The association has organized a cycle of webinars on the Lake Albano and the Lake of Nemi that have dealt with the rapid and alarming decrease in their water level, highlighting the causes, solutions and design ideas.
AIPIN – Associazione Italiana Per l'Ingegneria Naturalistica https://www.aipin.it/#:~:text=L'AIPIN%20%C3%A8%20un'associazione,le%20tecniche%20dell'ingegneria%20naturalistica AIPIN is a non-profit technical-scientific association with cultural and professional purposes founded with the aim of disseminating the methods and techniques of naturalistic engineering.

Assonautica Acque Interne Lazio e Tevere: ***Programmazione e controllo per lo sviluppo territoriale integrato e per il turismo sostenibile***
https://assonauticalaziotevere.it/
The activity of Assonautica Acque Interne Lazio e Tevere is aimed at creating synergies with local and territorial bodies and institutions on the issues of the environment, protection, enhancement, integrated development, sustainable tourism, navigation and water sports.

Articles

Il Porto Romano sulle rive del Lago Albano torna a vivere ***(The Roman Port on the shores of Lake Albano comes back to life)***
10 June 2022
https://www.metamagazine.it/il-porto-romano-sulle-rive-del-lago-albano-torna-a-vivere/

Castel Gandolfo, 29 maggio pulizia del Lago Albano con Carpfishing Castelli Romani ***(Castel Gandolfo, 29 May cleaning of Lake Albano with Carpfishing Castelli Romani)***
15 May 2022
https://www.castellinotizie.it/2022/05/15/castel-gandolfo-29-maggio-pulizia-del-lago-albano-con-carpfishing-castelli-romani/

S.O.S. Lago Albano di Castel Gandolfo. Consorzio di Bonifica Litorale Nord di Roma: ***Pronti a mettere a disposizione la competenza dei nostri tecnici. (S.O.S.Lake Albano of Castel Gandolfo. North of Rome Coastal Reclamation Consortium: Ready to make available the expertise of our technicians.)***
5 May 2022
https://www.osservatoreitalia.eu/s-o-s-lago-albano-di-castel-gandolfo-consorzio-di-bonifica-litorale-nord-di-roma-pronti-a-mettere-a-disposizione-la-competenza-dei-nostri-tecnici/

I danni causati dall'uomo all'ecosistema del Lago Albano ***(Manmade damage to the ecosystem of Lake Albano)***
4 April 2022
https://ilgiornaledellambiente.it/danni-causati-uomo-ecosistema-lago-albano/

Filmate possibili emissioni gassose sul Lago Albano ***(Possible gas emissions filmed on Lake Albano)***
8 December 2021
https://www.controluce.it/notizie/filmate-possibili-emissioni-gassose-sul-lago-albano/

Rafforzare le politiche di tutela su tutto il territorio lacustre dei Castelli Romani ***(The protection policies throughout the Castelli Romani lake territory have been strengthened)***
29 July 2021
https://golettaverde.legambiente.it/2021/07/29/rafforzare-le-politiche-di-tutela-su-tutto-il-territorio-lacustre-dei-castelli-romani/

Castel Gandolfo: Lago Albano più pulito grazie ai cittadini e alle associazioni ***(Castel Gandolfo: Lake Albano cleaner thanks to citizens and associations)***
13 April 2021
https://ilcaffe.tv/articolo/23103/lago-albano-piu-pulito-grazie-ai-cittadini

La crisi idrica dei laghi di Albano e Nemi – Attività di pianificazione sui Colli Albani negli ultimi vent'anni ***(The water crisis of the Lakes Albano and Nemi – Planning activities on the Colli Albani in the last twenty years)*** April 2021 – Professione geologo: Notiziario dell'ordine dei geologi del Lazio *(Professione geologo: newsletter of the order of geologists of Lazio Region)* extension://nhppiemcomgngbgdeffdgkhnkjlgpcdi/data/pdf.js/web/viewer.html?file=https%3A%2F%2Fgeologilazio.it%2Fwp-content%2Fuploads%2F2021%2F04%2FPG-62-web_new.pdf
Variazioni del livello del Lago Albano: informazioni dal fondale e ipotesi di ricostruzione storica ***(Changes in the level of Lake Albano: information from the seabed and hypothesis of historical reconstruction)*** April 2021 – Professione geologo: Notiziario dell'ordine dei geologi del Lazio *(Professione geologo: newsletter of the order of geologists of Lazio Region)* extension://nhppiemcomgngbgdeffdgkhnkjlgpcdi/data/pdf.js/web/viewer.html?file=https%3A%2F%2Fgeologilazio.it%2Fwp-content%2Fuploads%2F2021%2F04%2FPG-62-web_new.pdf
Festa della Madonna del Lago ***(Feast of the Madonna del Lago)*** 24 August 2019 https://www.castellinforma.it/home/event/92004
Lago Albano di Castel Gandolfo: Le iniziative dell'associazione ***Castel Gandolfo in movimento (Lake Albano of Castel Gandolfo: The initiatives of the Castel Gandolfo in motion movement)*** 28 July 2019 https://castelgandolfoinmovimento.blogspot.com/2019/07/lago-albano-di-castel-castel-gandolfo.html
Lago Albano ***osservato speciale*****. Arriva l'Istituto Superiore di Sanità** ***(Lake Albano under special scrutiny. Here comes the Higher Institute of Health)*** 7 March 2019 https://ilcaffe.tv/articolo/52857/lago-albano-osservato-speciale
Allarme a Castelgandolfo, i fondali del Lago Albano sono pieni di bombe ***(Alarm in Castel Gandolfo, thedepths of Lake Albano are full of bombs)*** 11 November 2016 https://www.ilmattino.it/primopiano/cronaca/castelgandolfo_allarme_bombe_fondali_pieni-2074934.html?refresh_ce
Lago Albano: dentro l'antico emissario ***(Lake Albano: inside the ancient emissary)*** Luglio/Agosto 2016 – Archeologia Viva n. 178 https://www.archeologiaviva.it/4496/lago-albano-dentro-lantico-emissario/
Albano naviga in cattive acque ***(Albano is in dire straits)*** 13 November 2012 https://comune-info.net/albano-naviga-in-cattive-acque/
Albano Laziale Emissario del lago ***(Albano Laziale Emissary of the lake)*** https://www.tesoridellazio.it/tesori/albano-laziale-emissario-del-lago/

È realtà il *Contratto di Falda Lago Albano, Nemi e per il fiume Incastro*. Enti e Associazioni insieme per salvare i laghi dei Castelli Romani *(The Aquifer Contract of Lake Albano, Nemi and for the Incastro river has become reality. Bodies and associations join forces to save the Castelli Romani lakes)* https://www.castellinotizie.it/2021/03/02/e-realta-il-contratto-di-falda-lago-albano-nemi-e-per-il-fiume-incastro-enti-e-associazioni-insieme-per-salvare-i-laghi-dei-castelli-romani/
Lago Albano *(Lake Albano)* https://www.ricominciodaroma.it/item/lago-albano/

REFERENCES

[1] Patera, A. & Fabbri, A.G., Analisi della pericolosità di frana dei versanti interni del Lago Albano (Landslide hazard assessment of the internal slopes of Lake Albano). *Rapporti Tecnici INGV*, Rome (in press).

[2] Barberi, F., Chelini, F., Marinelli, G. & Martini, M., The gas cloud of Lake Nyos (Cameroon, 1986): Results of the Italian technical mission. *Journal of Volcanology and Geothermal Research*, **39**, pp. 125–134, 1989.

[3] Funiciello, R., Giordano, G., De Rita, D., Carapezza, M.L. & Barberi, F., L'attività recente del cratere del Lago Albano di Castelgandolfo. *Rendiconti dell'Accademia dei Lincei (Scienze Fisiche e Naturali)*, **9**(13), pp. 113–143, 2002.

[4] Carapezza, M.L. & Tarchini, L., Magmatic degassing of the Alban Hills volcano (Rome, Italy): Geochemical evidence from accidental gas emission from shallow pressurized aquifers. *Journal of Volcanology and Geothermal Research*, **165**, pp. 5–16, 2007.

[5] Bozzano, F., Mazzanti, P., Anzidei, M., Esposito, C., Floris, M., Bianchi Fasani, G. & Esposito, A., Slope dynamics of Lake Albano (Rome, Italy): Insights from high resolution bathymetry. *Earth Surface Processes and Landforms*, **34**, pp. 1469–1486, 2009.

[6] Mazzanti, P., Bozzano, F. & Esposito, C., Submerged landslide morphologies in the Albano Lake (Rome, Italy). *Submarine Mass Movements and Their Consequences*, eds V. Lykousis, D. Sakellariou & J. Locat, Springer: Dordrecht, 2007.

[7] Anzidei, M., Esposito, A. & De Giosa, F., The dark side of the Albano crater lake. *Annals of Geophysics*, **49**, pp. 1275–1287, 2007.

[8] Cruden, D.M. & Varnes, D.J., Landslide types and processes. *Landslides Investigation and Mitigation*, eds A.K. Turner & R.L. Shuster, National Research Council, Transportation Research Board: Washington, DC. Special Report, **247**, pp. 36–75, 1996.

[9] Mulder, T. & Cochonat, P., Classification of offshore mass movements. *Journal of Sedimentary Research*, **66**(1), pp. 43–57, 1996.

[10] Chung, C.J. & Fabbri, A.G., Representation of geoscience data for information integration. *Natural Resources Research*, **2**, pp. 122–139, 1993.

[11] Fabbri, A.G. & Chung, C.J., How credible is my hazard map? Dissecting a prediction pattern of landslide susceptibility. *WIT Transactions of Engineering Sciences*, vol. 121, WIT Press: Southampton and Boston, pp. 3–19, 2018. DOI: 10.2495/RISK180011.

[12] Fabbri, A.G. & Patera, A., Spatial uncertainty of target patterns generated by different prediction models of landslide susceptibility. *Applied Sciences*, **11**, p. 3341, 2021.

[13] Chung, C.J. & Fabbri, A.G., Prediction models for landslide hazard using fuzzy set approach. *Geomorphology and Environmental Impact Assessment*, eds M. Marchetti & V. Rivas, Balkema: Rotterdam, pp. 31–47, 2001.

[14] Chung, C.F., Computer program for the logistic model to estimate the probability of occurrence of discrete events. *Geological Survey of Canada Paper*, 78-11, pp. 1–23, 1978.

[15] Davis, J.C., Davis, J.C., Chung, C.F. & Ohlmacher, G.C., Two models for evaluating landslide hazards. *Computers and Geosciences*, **32**, pp. 1120–1127, 2006.

[16] Chung, C.J. & Fabbri, A.G., Validation of spatial prediction models for landslide hazard mapping. *Natural Hazards*, **30**, pp. 451–472, 2003.

[17] Fabbri, A.G., Cavallin, A., Patera, A., Sangalli, L. & Chung, C.J., Comparing patterns of spatial relationships for susceptibility prediction of landslide occurrences. *Advancing Culture of Living with Landslides: Advances in Landslide Science*, eds M. Mikoš, B. Tiwari, Y. Yin & K. Sassa, Springer: Switzerland, pp. 1135–1144, 2017.